■成果報告

行政院國家科學委員會補助專題研究計畫

□期中進度報告

強關聯量子物質之材料、界面、與其衍生性物理特性研究--子計畫二:

量子體物性的基礎研究與控制(第三年)

計畫類別:□個別型計畫 ■整合型計畫

計畫編號: NSC 98-2112-M-009-005-MY3

執行期間:98年8月1日至102年7月31日

計畫主持人:林俊源

計畫參與人員:溫智匡、施沛姍

成果報告類型(依經費核定清單規定繳交):□精簡報告 ■完整報告

處理方式:除產學合作研究計畫、提升產業技術及人才培育研究計畫、列管計畫及下列情形者,得立即公開查詢

執行單位:國立交通大學物理研究所

中 華 民 國 102 年 6 月 19 日

Part-1

X-ray absorption near edge spectroscopy (XANES) was employed to study the valence and spin degree of freedom of transition metal ions in materials.

For the case of $Ni(NO_3)_2$, the Ni *L*-edge spectrum indicates divalence nickel in $Ni(NO_3)_2$ compounds. Combined with the theoretical calculations, we confirm that the divalent nickel exhibits the high spin state (S=1) in $Ni(NO_3)_2$. In the study, NiO (Ni^{2+}, S=1) was used as the standard sample. The spectrum shape differences between NiO and $Ni(NO_3)_2$ come from the different local environments.

Moreover, we measured room temperature Mn *K*, $L_{2,3}$-edge and Co *K*, $L_{2,3}$-edge and temperature dependent Co $L_{2,3}$-edge XANES spectra in $PrSrCoMnO_6$ double perovskites. Our spectra show the Co^{3+}/Mn^{4+} ionic state in $PrSrCoMnO_6$. With the help of theoretical calculations, we found that the crystal field in CoO_6 octahedral is close to the HS-LS transition boundary. The crystal structure in $PrSrCoMnO_6$ was solved at T=300 K and T=12 K, respectively. $PrSrCoMnO_6$ shows an unusual lattice change at low temperatures. The lattice volume and the average Mn-O bond length decrease, but the average Co-O bond length increases at low temperatures. We also find there is a close relationship between CoO_6 local environment and Co *L*-edge spectra line shape. The temperature dependent Co *L*-edge XAS spectra of $PrSrCoMnO_6$ obviously demonstrate the spin state variation with T, which can be described as the combination of a LS ground state and the triply degenerate HS first excited states.

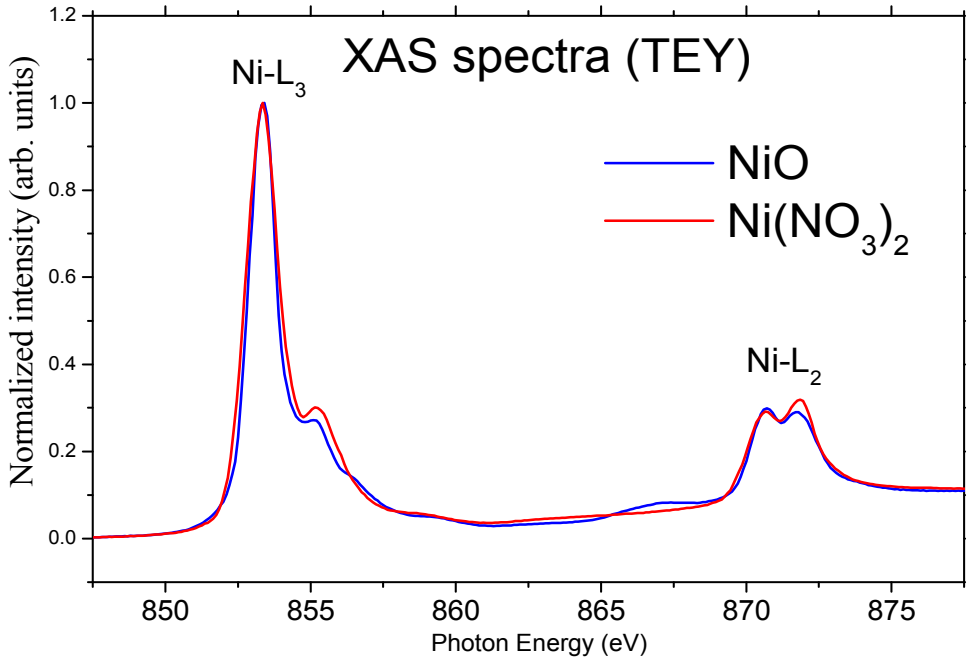

Fig. 1. Nickel $L_{2,3}$ edge XAS data in TEY.

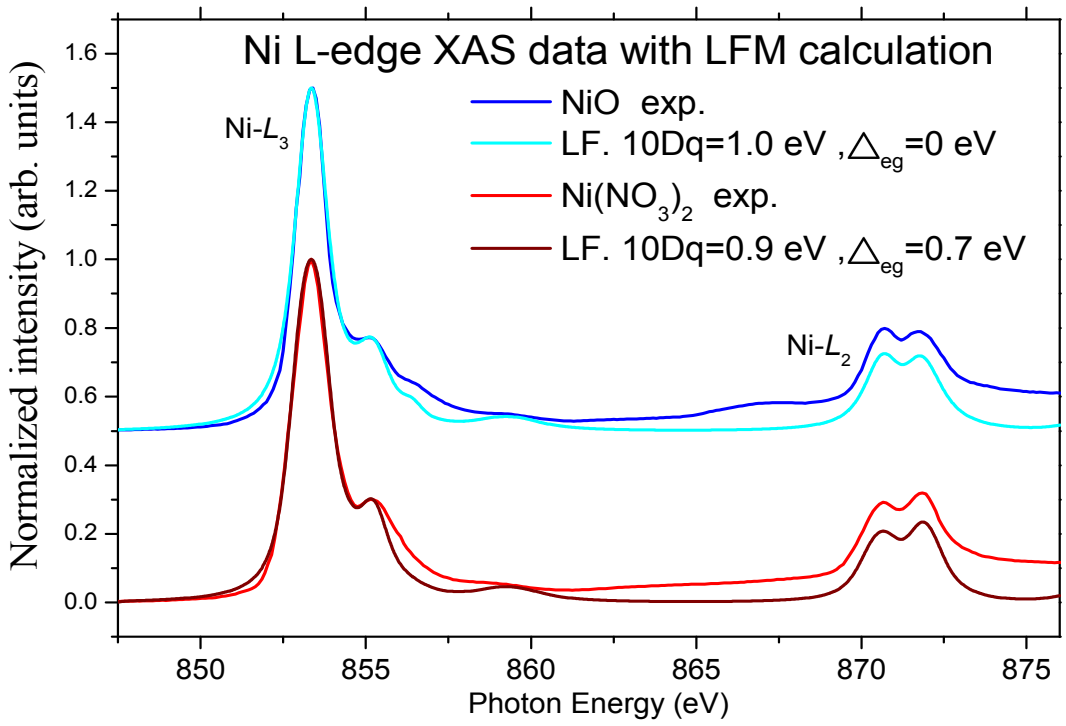

Fig. 2. Nickel $L_{2,3}$ edge XAS data with ligand field model calculations.

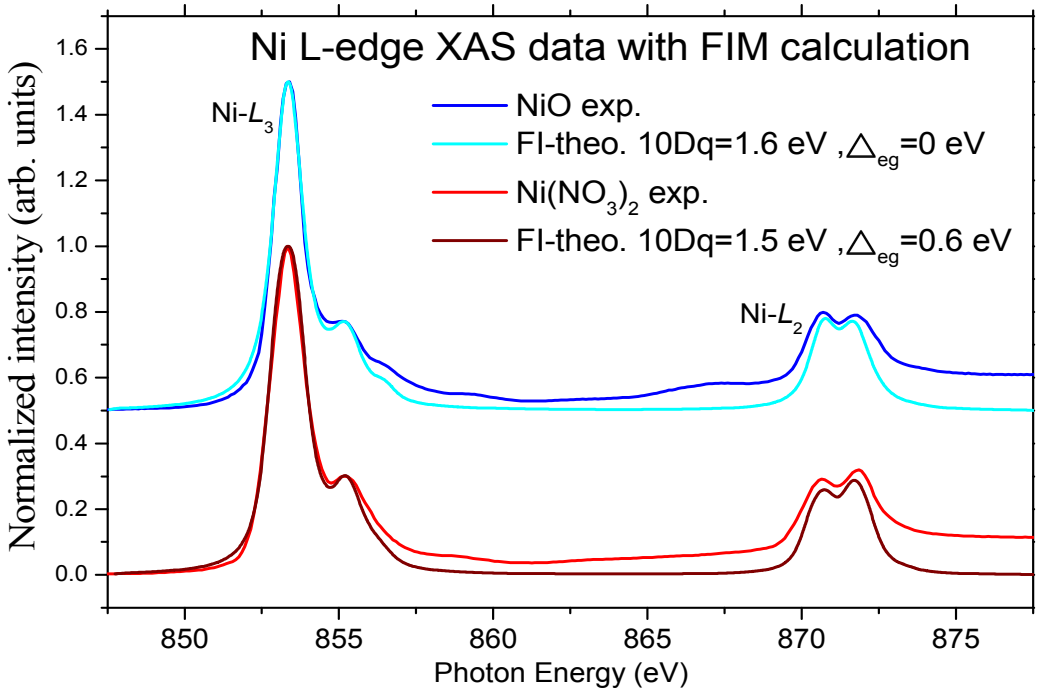

Fig. 3. Nickel $L_{2,3}$ edge XAS data with free ion model calculations.

the XAS spectra shows the divalence nickel in $Ni(NO_3)_2$ compound. Combine with the theoretical calculation, we assume that the divalence nickel shows a high spin state S=1 in $Ni(NO_3)_2$, same as NiO. The spectrum shape differences between NiO and $Ni(NO_3)_2$ come from the different local environments.

On the other hand, very recently, O. Volkova et al. [1] measured magnetization measurement under magnetic field as shown in Fig. 3, the obtained value of saturation moment amounts about 2.03 μ_B/f.u. which is very close to the theoretical one $M_S = ngS\mu_B = 2.15\ \mu_B$/f.u. for Ni^{2+}, S=1, which is consistent to our simulations.

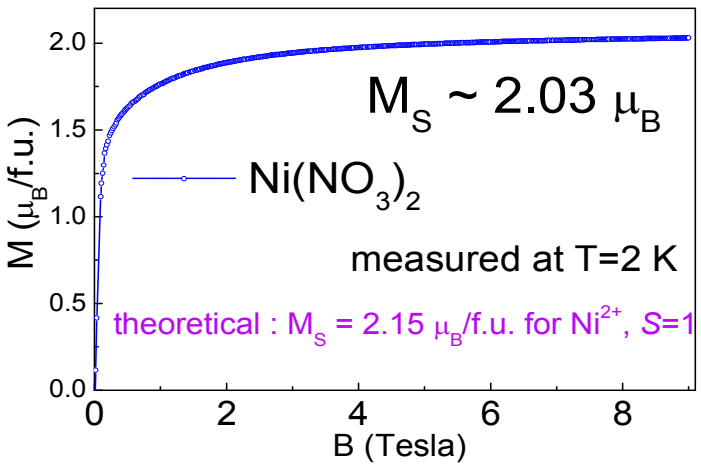

Fig. 3. Magnetization measurement of $Ni(NO_3)_2$ At 2 K under magnetic field.[1]

Room temperature Mn *L*-edge XAS data was recorded in total electron yield (TEY) mode (see Fig.4). In the previous work, which shows the $PrSrCoMnO_6$ sample has a similar spectra shape and energy position with MnO_2, we infer that the valence on manganese ion should be Mn^{4+}.

Room temperature Mn *K*-edge XAS was recorded in the transmission mode. The edge position is sensitive to Mn valence in the *K*-edge spectra, which also represents the Mn^{4+} in PrSrCoMnO6 sample (see Fig.5), same as those Mn^{4+} in Eu_2CoMnO_6 and La_2CoMnO_6 double perovskite**[**2,3,**4]**.

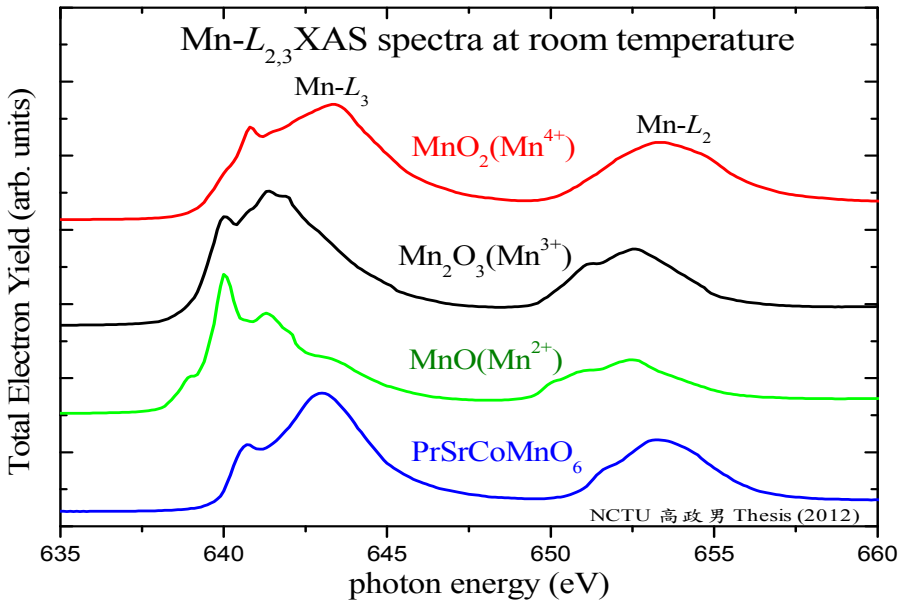

Fig. 4 Mn *L*-edge XAS data in TEY mode

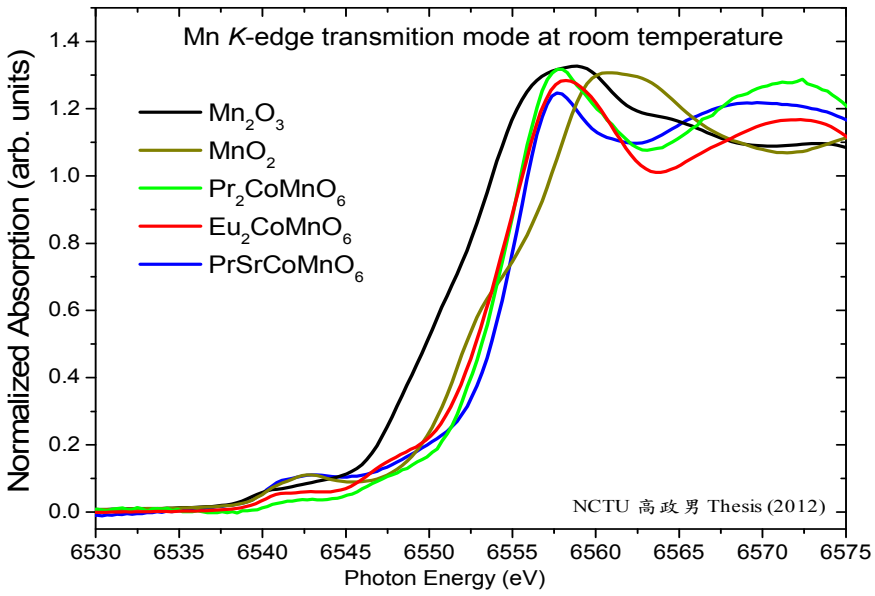

Fig. 5 Mn *K*-edge XAS data in transimission mode

In Co *K*-edge, room temperature XAS was recorded in the transmission mode from BL.17C in NSRRC Taiwan, as shown in Fig.6. The K-edge XAS spectra is very sensitive to the valence of transition metal ions. Compare with other reference spectra, we find the $PrSrCoMnO_6$ spectrum is very similar to $EuCoO_3$, and we infer that the cobalt ions are also trivalence in $PrSrCoMnO_6$ sample.

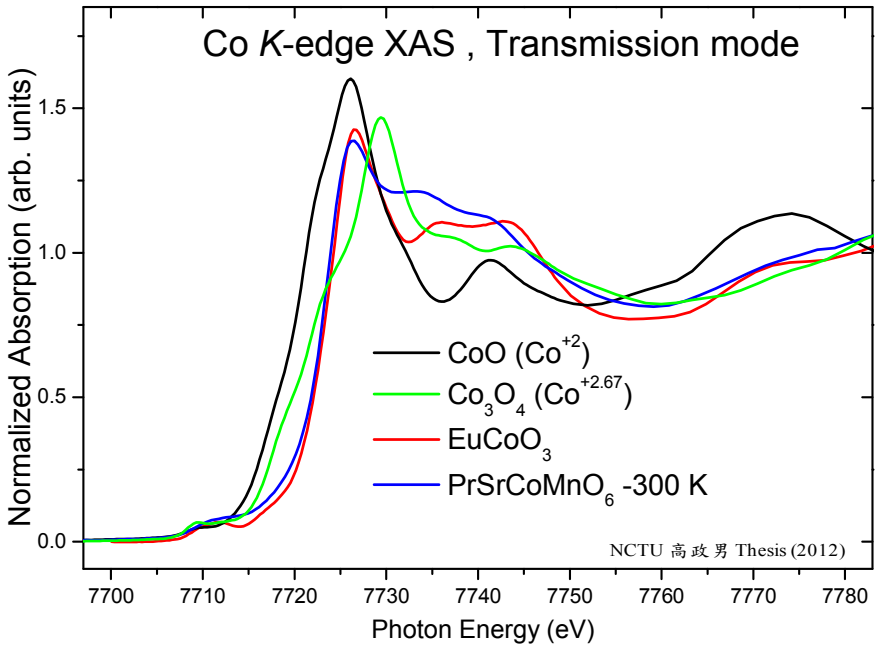

Fig.6. Co K-edge XAS spectra in transmission mode

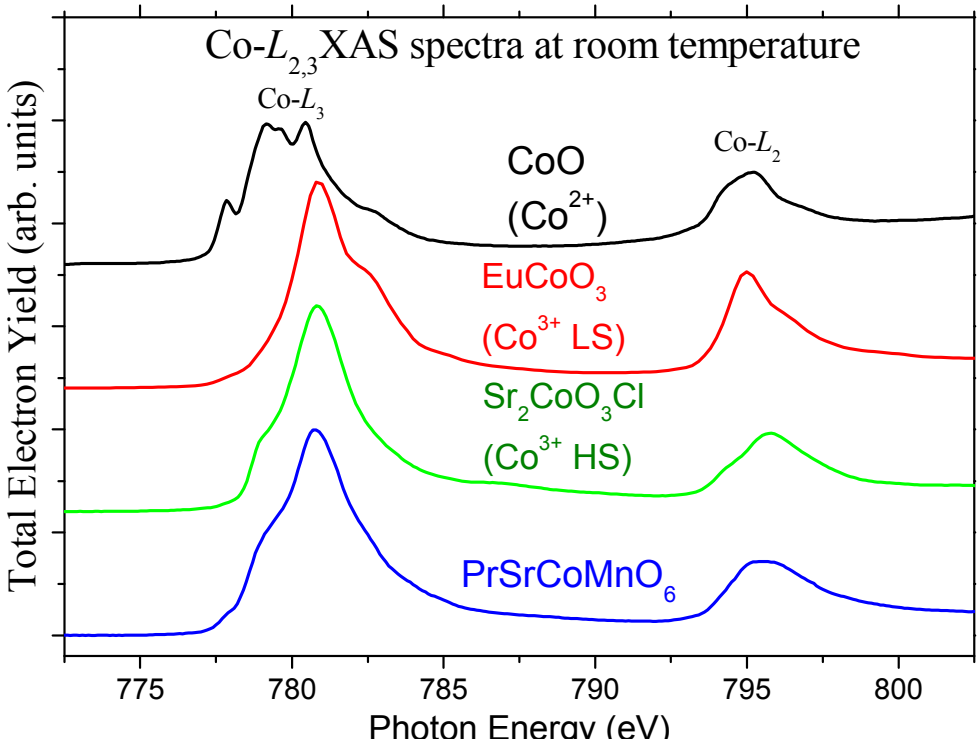

Fig. 7 Co *L*-edge XAS data

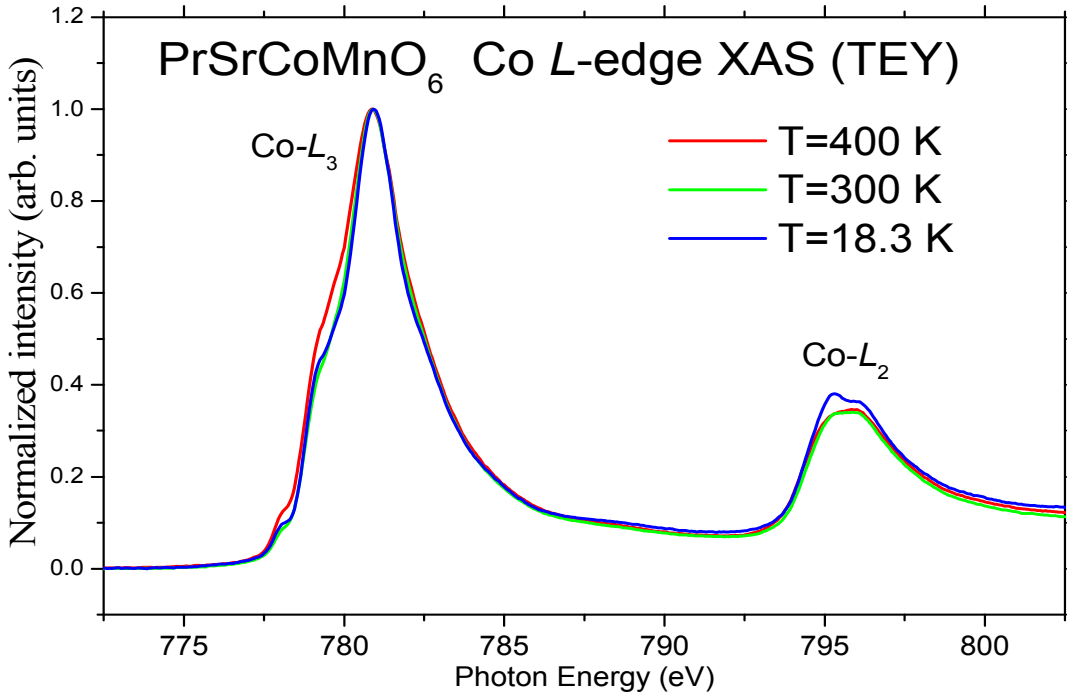

Fig. 8 Temperature dependent Co *L*-edge XAS spactra on $PrSrCoMnO_6$ sample

We focus on the L_3-edge first, there shows a shoulder characteristic in the lower energy range, which is the contribution from Co^{3+} HS state. As the temperature increasing, the shoulder intensity also increases. We infer that the HS population increases with temperature increasing. Now turn to the L_2-edge, there shows a peak at 795eV which come from Co^{3+} LS spectra. As the temperature increasing, we saw the peak intensity become lower. We infer that the LS population decreases with the temperature increasing, this result consists with that in the L_3-edge. Up to now, we assume that the Co^{3+} ions in $PrSrCoMnO_6$ sample is an HS-LS mixed-spin state system, and the HS state presence more at higher temperature.

We infer that the cobalt ion in $PrSrCoMnO_6$ sample is a HS-LS mixed system, which has a LS ground state and the triply degenerate HS 1st exciting states, and the higher HS population, which come from the thermal excitation, presence more at high temperature.

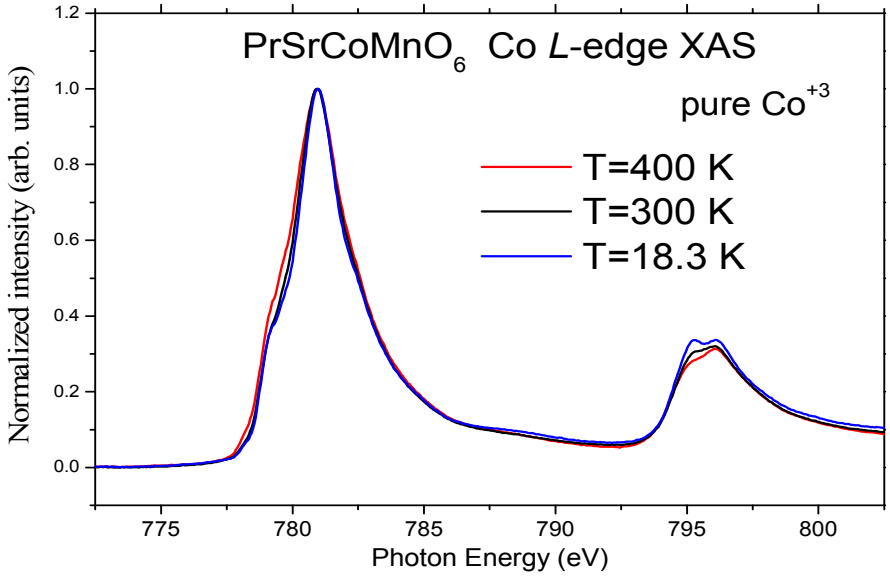

Fig 9 Temperature dependent Co^{3+} *L*-edge XAS spectra.

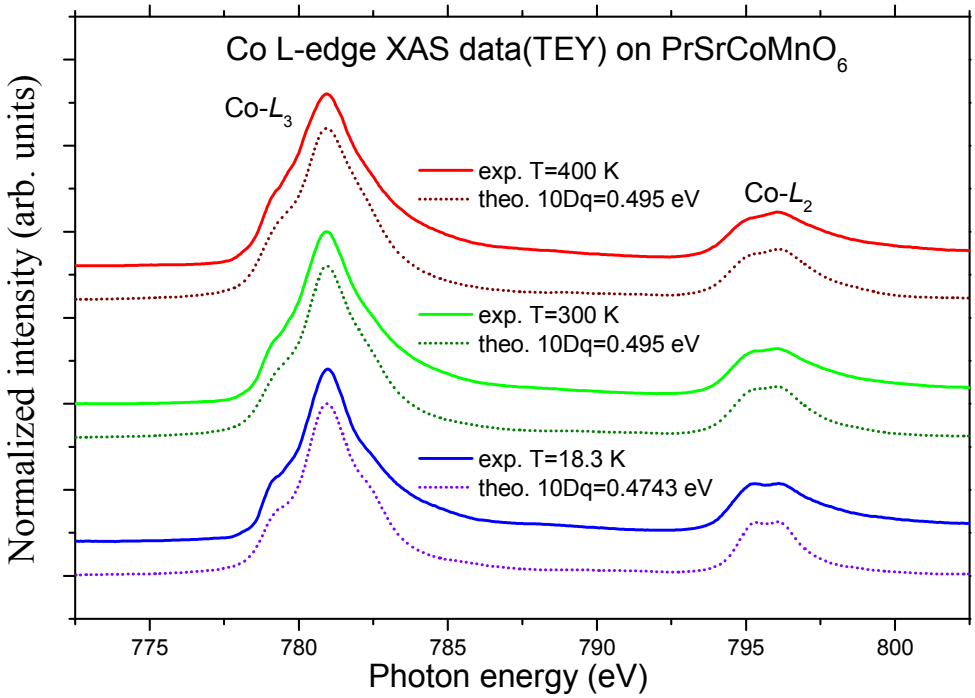

Fig 10 Co L-edge XAS experiment data with theoretical calculation (setting the fitting temperature parameter equals to real experiment conditoin).

At the end, we also fit the room temperature Co L-edge XAS spectra in different samples. The fitting parameter 10*Dq*=0.495 eV shows the best fit to $PrSrCoMnO_6$, while the 10*Dq*=0.52 eV can fit $LaCoO_3$ well and 10*Dq*=0.54 eV can fit $EuCoO_3$ at room temperature (see Fig.11). Compare the average Co-O bond length with the fitting parameter 10*Dq* in each sample, we obviously see the fitting parameter 10Dq (point charge crystal field in octahedral symmetry) decreasing with the increasing of average Co-O bond length as shown in Fig.12. The gray dash curve shows the linear fit of room temperature cases, and the light blue curve shows the Co^{3+} ground state HS-LS transition boundary 10*Dq*=0.47258 eV calculated from XTLS software.

Compare with $EuCoO_3$ and $LaCoO_3$, $PrSrCoMnO_6$ has the largest average Co-O bond length and the smallest crystal field on Co^{3+} ions in the CoO_6 coordination, and the crystal field in $PrSrCoMnO_6$ is much closer to the HS-LS transition boundary, especially in the low temperature.

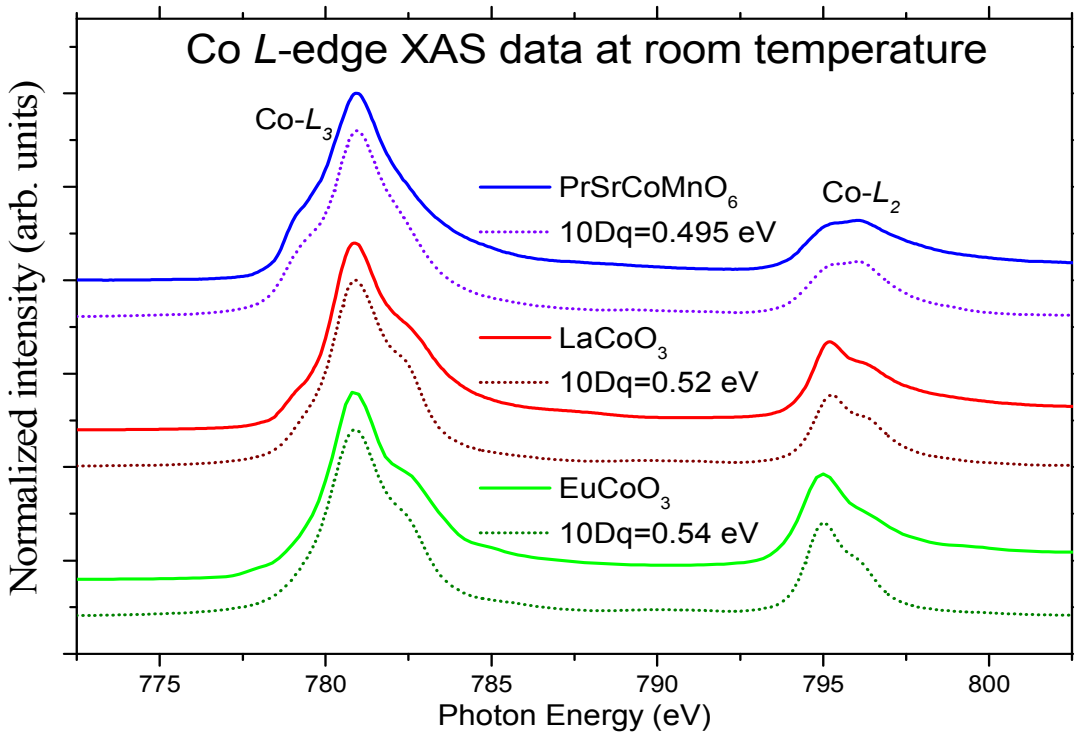

Fig. 11 Co *L*-edge XAS spectra with theoretical calculation

Sample	Average Co-O (Å)	fitting 10*Dq* (eV)
$EuCoO_3$	1.9297	0.54
$LaCoO_3$	1.932(1)	0.52
$PrSrCoMnO_6$ room-T	1.937(101)	0.495
$PrSrCoMnO_6$ low-T	1.980(57)	0.4743

Table 1 The comparison of average Co-O bond length with the fitting parameter 10*Dq* in different Co^{3+} samples.

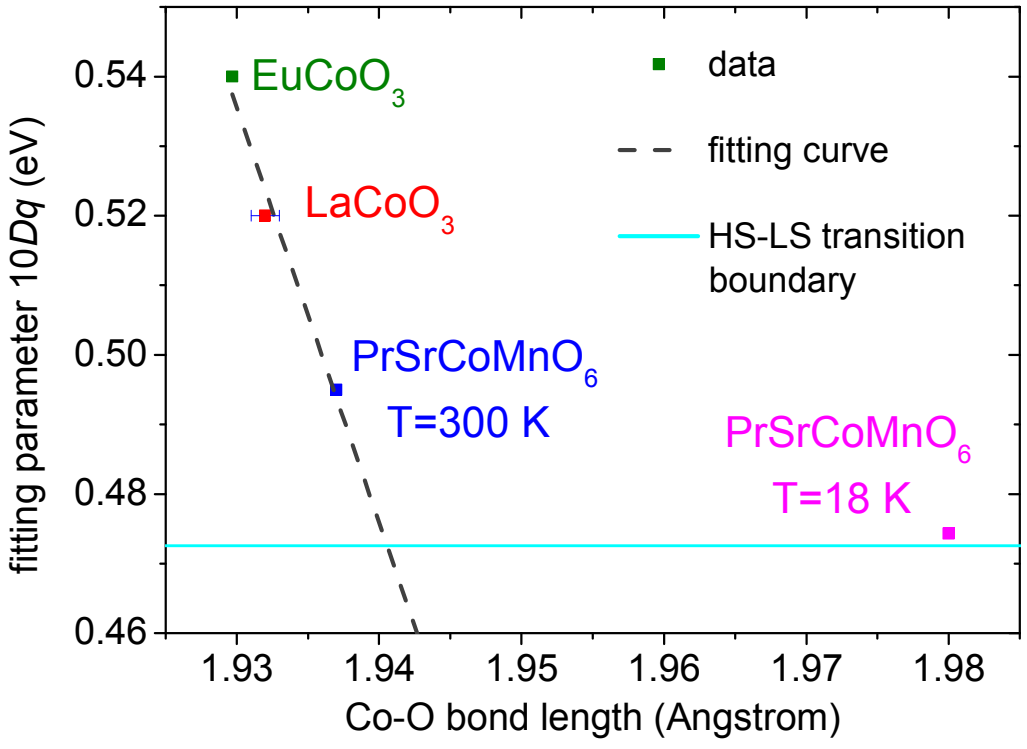

Fig. 12 The relationship between the fitting parameter 10*Dq* with the average Co-O bond length in different Co^{3+} samples.

參考條目

[1] O. Volkova, E. Deeva, I. Morozov, V. Mazurenko, I. Solovyev, J.-Y. Lin, C.K. Wen, R. Klingeler, B. Büchner, and A. Vasiliev, unpoblished

[2] N. Vasiliev, O. S. Volkova, L. S. Lobanovskii, I. O. Troyanchuk, Z. Hu, L. H. Tjeng, D. I. Khomskii, H.-J. Lin, C. T. Chen, N. Tristan, F. Kretzschmar, R.Klingeler,6and B. Büchner, PHYSICAL REVIEW B 77, 104442 (2008).

[3] T. Burnus , O. S. Volkova, L. S. Lobanovskii, I. O. Troyanchuk, Z. Hu, L. H. Tjeng, D. I. Khomskii, H.-J. Lin, C. T. Chen, N. Tristan, F. Kretzschmar, R. Klingeler, and B. Büchner, PHYSICAL REVIEW B 77, 125124 (2008).

[4] 高政男，碩士論文，”以吸收光譜研究鈣鈦礦結構中鈷氧化物自旋態與鈷離子價數”，國立交通大學，(2012)。

Part-2

In 2004, E. Bauer[1] discovered the first heavy fermion superconductor without inversion symmetry. According to the literature, $CePt_3Si$ is not excluding spin-triplet pairing completely. At the same year, from the theatrical calculation[2], the superconductivity in non-centrosymmetric material exhibits intriguing properties due to a spin degeneracy splitting of Fermi surface is observed by spin-orbit coupling. Superconducting order parameter does not obey parity conservation anymore, it becomes possible for comprising of a mixing of spin-singlet and spin-triplet that is also known as a simplest form in mixture of *s*-wave and *p*-wave. In general, reducing the effect of Coulomb repulsion may display nodes in energy gap.

The strong electronic correlation system involves *f*-electron, like $CePt_3Si$ and pressure-induced superconductors, e.g. CeTX_3 (T=Co, Rh, Ir; X=Si, Ge) and UIr, indeed, the presence of an unconventional order parameter in these non-centrosymmetric materials. For $CePt_3Si$, in particular, line node in energy gap is proven from the experiment of the thermal conductivity[3], penetration depth[4] and specific heat[5]. On the other hand, these non-centrosymmetric superconductors without heavy fermion features are attracted more attention, the pairing state of most weakly electronic correlation systems are *s*-wave which include $Mg_{12-\delta}Ir_{19}B_{16}$[6][7] R_2C_{3-y} (R=La, Y), T_2Ga_9 (T=Rh, Ir, Pt), $LaPt_3Si$, $AMSi_3$ (A=Ba, Ca, La; M=Rh, Ir, Pt), $Li_2(Pd_{1-x}Pt_x)_3B$, Ru_7B_3, $Nb_{0.18}Re_{0.82}$[8]Re_3W[9][10] $Re_{24}Nb_5$[11]owever, there are some agreements in order parameter: for instance, evidences provide different results for R_2C_{3-y} (R=La, Y)[17][18], BiPd, Mo_3Al_2C4[12-14], $Mg_{12-\delta}Ir_{19}B_{16}$[19][20], and $Li_2(Pd_{1-x}Pt_x)_3B$ beyond the component x=0.8.

Such strong spin-orbit coupling system as topological insulators, the solid has bulk insulator states and surface conducting states consisting of Majorana fermions[21], which is its own antiparticle that is characteristic of Bosons, and expected to appear at the edge of the vortex in topological insulators. Most of the theoretical proposals for the Majorana fermions are based on *p*-wave pairing in the one-dimensional spinless fermions and the *p*+*ip* pairing superconductor[22]. So far, some groups suggest the mixing pairing states exist due to impurity effect enhances spin-orbit coupling[7][14], nevertheless, no one actually finds it in superconductors. Thus, we are going to search for the proportion of *p*-wave in non-centrosymmetric superconductors with binary α-Mn structure by measuring specific heat.

Specific Heat Result

$Re_{24}Ti_5$

The specific heat data in Figure 1 lotted as C/T *vs.* T^2 shows the superconducting state and normal state. The normal specific heat usually is expressed as sum of electronic contribution and phonon contribution,

$$C_n(T) = C_e(T,H) + C_{lattice}(T) = \gamma_n T + \beta T^3 + \delta T^5 \quad (4\text{-}1)$$

where $\gamma_n T$ represents the electronic term due to free charge carriers, and $\beta T^3 + \delta T^5$ depicts phonon contribution is assumed to be independent of the magnetic field.

It is found an extrapolation of fitting normal state to $T = 0\ \mathrm{K}$, then we can determine the $\gamma_n = 111.8\ \mathrm{mJ/mol\,K^2}$ and the other fitting parameters. We also calculated Debye temperature $\theta_D = 343\ \mathrm{K}$ from equation (2-12).

We can directly observe the transition temperature $T_c = 5.74\ \mathrm{K}$ and dimensionless specific jump $\Delta C/\gamma_n T_c = 1.60$ in superconducting state which reveals an incontinuous phenomenon in specific heat. $\Delta C/\gamma_n T_c$ is larger than the theoretical value of 1.43 that suggests a moderately enhanced electron-phonon coupling.

In the following function[16], we can estimate the electron-phonon constant λ_{ep}.

$$\Delta C/\gamma_n T_c = 1.43 + 0.942\lambda^2 - 0.195\lambda^3 \quad (4\text{-}2)$$

According to McMillan model, for weak coupling $\lambda \ll 1$, for weak and intermediate coupling $\lambda < 1$, and for strong coupling $\lambda > 1$. Therefore, the present $\lambda_{ep} = 0.45$ value implies that our samples are a moderate coupling superconductor rather than a weak coupling one. The result is consistent with specific jump.

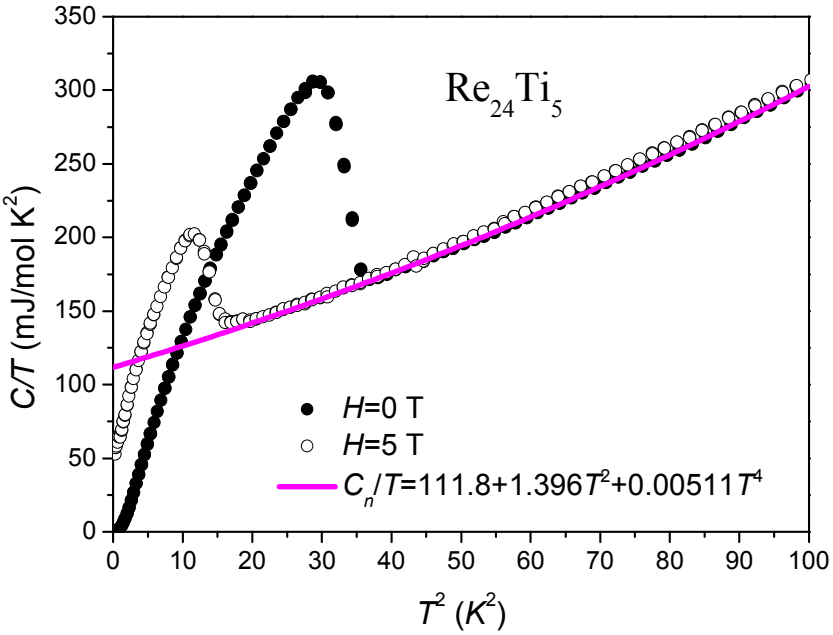

Figure 1 Specific heat of $Re_{24}Ti_5$ and the pink line is its normal state.

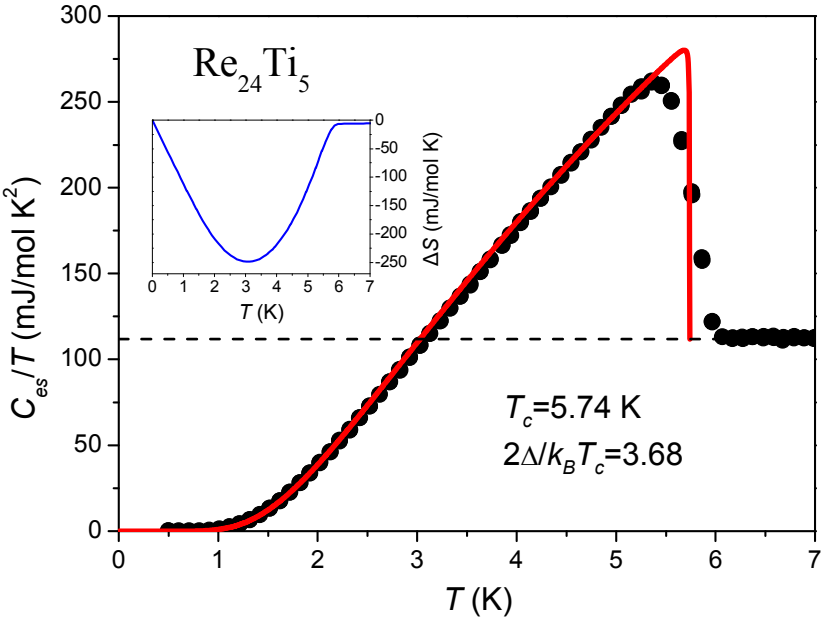

Figure 2 The black solid is superconducting electronic conurbation of $Re_{24}Ti_5$ with isotropic *s*-wave fitting(red line).

Inset: the entropy conservation for the superconducting phase transition.

The superconducting electronic contribution is shown in Figure 2, we calculate it by the formula, $\Delta C(T) = C(T, H = 0\ \mathrm{T}) - C_n(T)$ and which can be described by

s-wave. In addition, superconducting phase transition is second order that has to obey entropy conservation $S = \int_0^{T_c} (\Delta C/T) dT$ around transition temperature.

In the light of specific heat data(which in reference 27), we found the critical temperature for each corresponding magnetic field and plotted them as Figure 3.

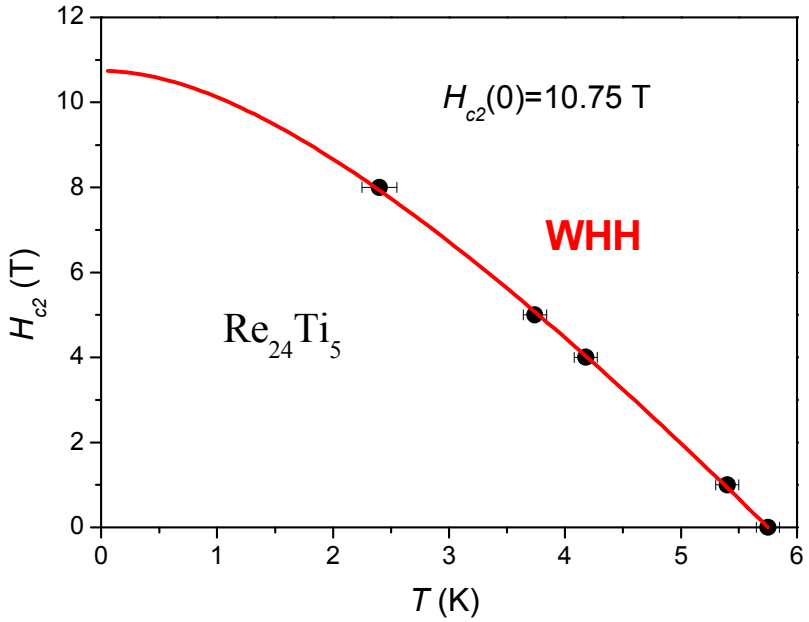

Figure 3 Temperature dependence of upper critical fields of $Re_{24}Ti_5$[15], and the red curve is from Werthamer-Helfand-Hohenberg (WHH) theory.$Re_{21.75}Ta_{7.25}$

In Figure 4, the specific heat of $Re_{21.75}Ta_{7.25}$ plotted as C/T *vs.* T^2. The normal state is derived from equation (4-1) and the superconducting state is also obtained by the formula, $\Delta C(T) = C(T, H = 0\ \mathrm{T}) - C_n(T)$ which complies with entropy balance around transition temperature as well as shows in Figure 5 with *s*-wave fitting.

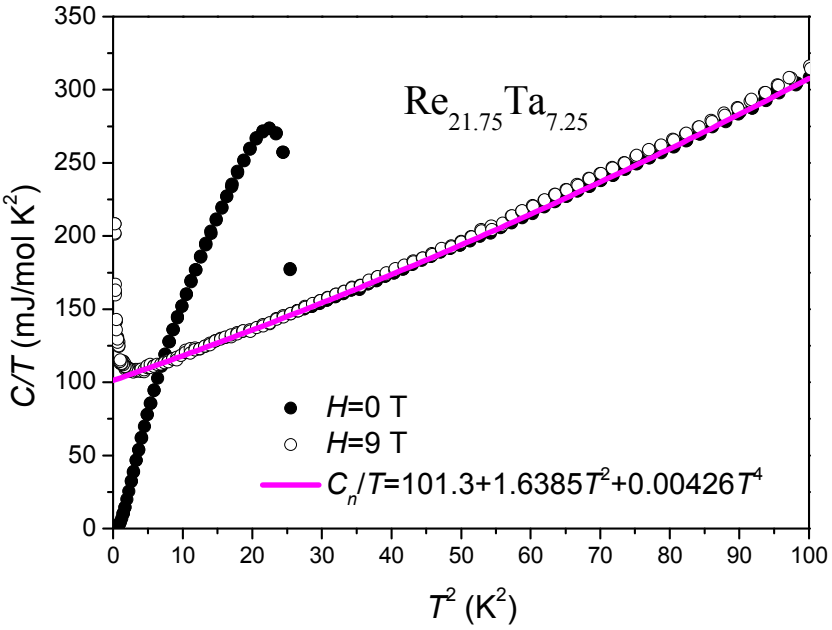

Figure 4 The specific heat of $Re_{21.75}Ta_{7.25}$, and the pink line is the normal state.

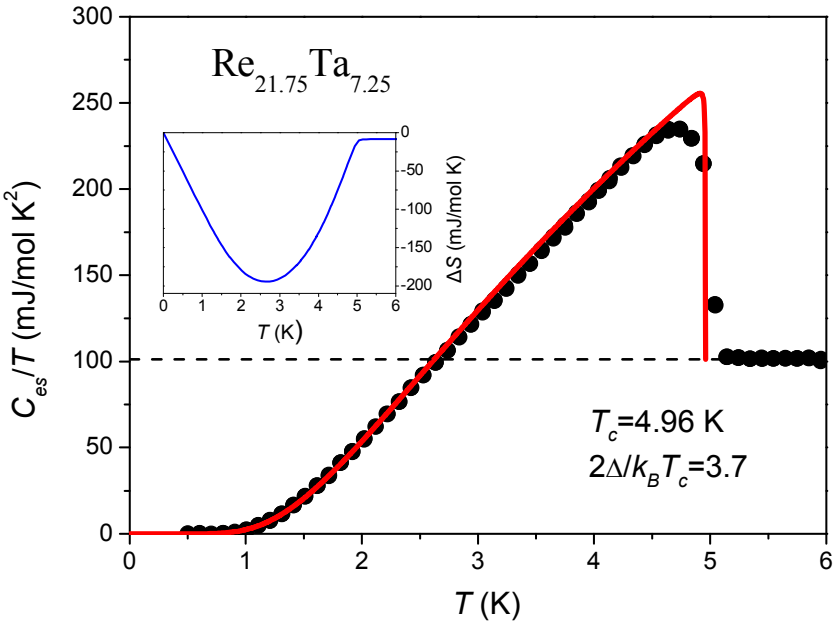

Figure 5 The black solid is superconducting electronic conurbation of $Re_{21.75}Ta_{7.25}$ with isotropic *s*-wave fitting(red line).

Inset: the entropy balance for the superconducting phase transition.

By the above fitting result and equation (2-12), (4-2), it is easy to know the

transition temperature $T_c = 4.96$ K, Debye temperature $\theta_D = 325$ K, furthermore, specific jump $\Delta C/\gamma_n T_c = 1.52$ and electron-phonon coupling $\lambda_{ep} = 0.32$.

4.1.3 $Re_{24.9}Hf_{4.1}$

Follow the discussion of section 4.1.1 and 4.1.2, the specific heat of $Re_{24.9}Hf_{4.1}$ is plotted as C/T *vs.* T^2 and shown in Figure 6. The normal state is fitted by equation (4-1) and the electronic superconducting specific heat is fitted by *s*-wave, further, the second phase transition compels the existence of entropy conversation, as Figure 7 with different order parameter. On the basis of equation (2-12) and (4-2), we obtained following parameters of $Re_{24.9}Hf_{4.1}$: $T_c = 5.54$ K, $\theta_D = 335$ K, then, $\Delta C/\gamma_n T_c = 1.55$ and $\lambda_{ep} = 0.37$.

For the sake of accurately analyzing $Re_{24.9}Hf_{4.1}$, we measured its specific heat with different magnetic field. There are two ways to find the upper critical field at zero temperature, one is using the applied magnetic field *vs.* transition temperature, and the other one is plotting γ *vs.* magnetic field. As Figure 8, first, taking a interception of linear fit to $T = 0$ K in a figure as C/T *vs.* T^2 below 0.9 K except for $H = 7$ T, and the upper critical field is the intersection point between the linear fit of $\gamma(H)$ which passing through origin and $\gamma_n = 107$ mJ/mol K^2. In another way, we made use of Werthamer-Helfand-Hohenberg (WHH) theory without impurity scattering ($\alpha = 0$) and spin-orbit scattering ($\lambda = 0$) to fit the data of the applied magnetic field *vs.* its corresponding transition temperature, and it is shown in Figure 9.

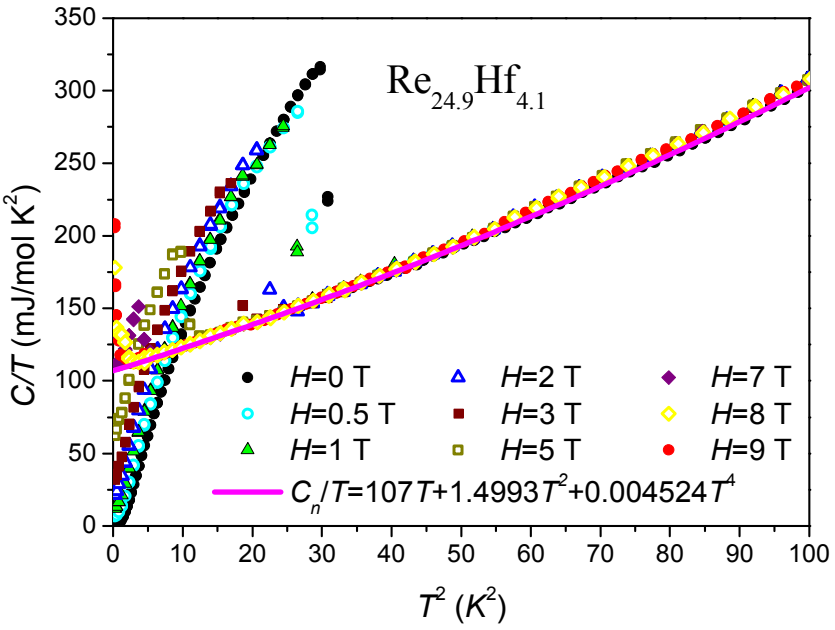

Figure 6 The specific heat of $Re_{24.9}Hf_{4.1}$, and the pink line is the normal state.

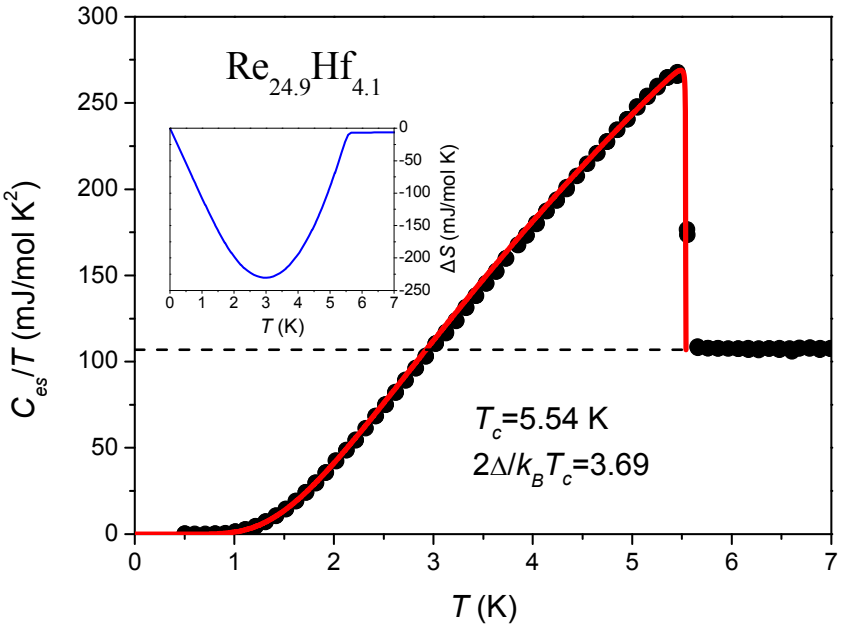

Figure 7 The black solid is superconducting electronic conurbation of $Re_{24.9}Hf_{4.1}$ with isotropic *s*-wave fitting(red line).

Inset: the entropy conservation for the superconducting phase transition.

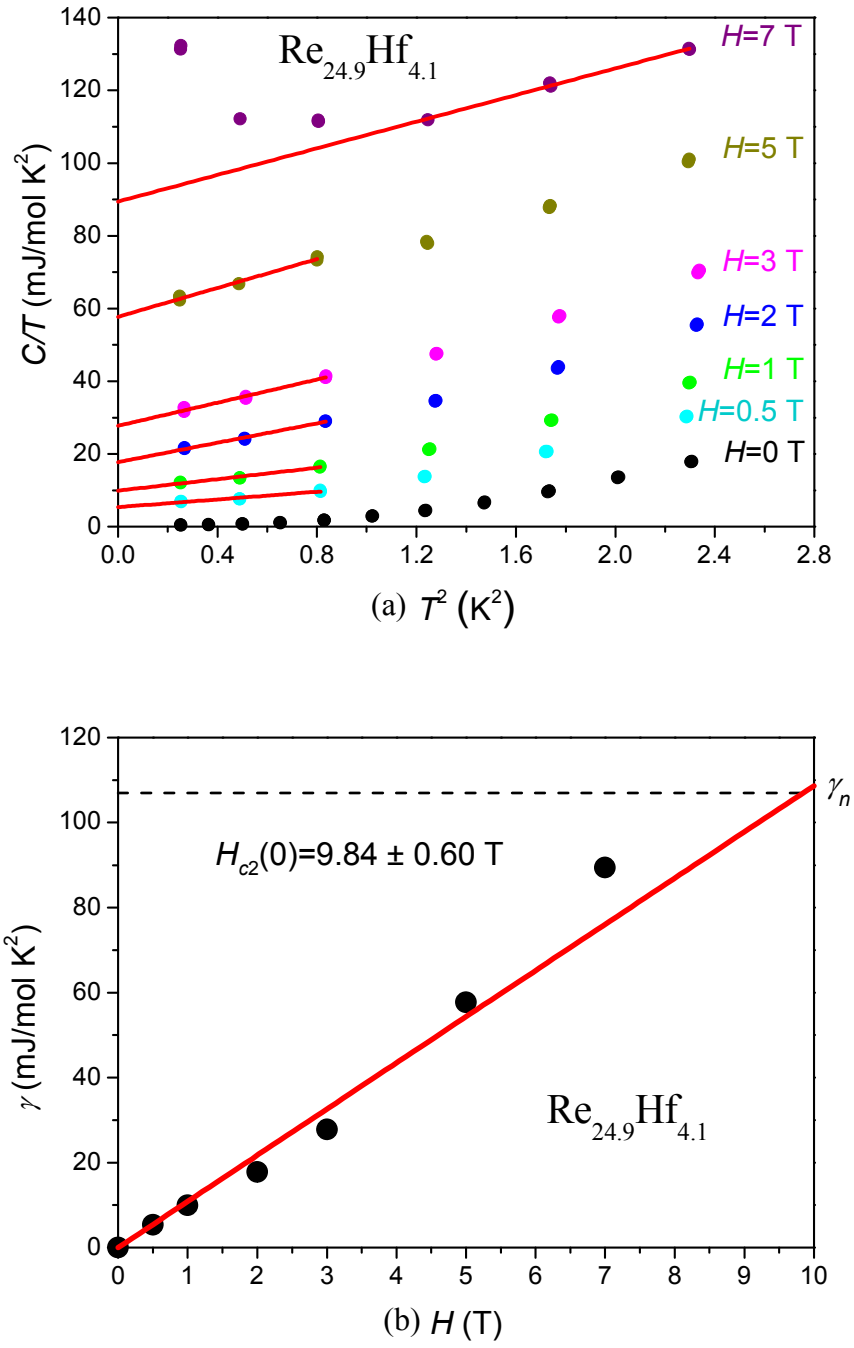

Figure 8 For $Re_{24.9}Hf_{4.1}$, (a) $\gamma(H)$ has been derived from the liner extrapolation of data at low temperatures using C/T *vs.* T^2. (b)Magnetic field dependence of electronic specific heat coefficient, where the dash line is γ_n and the red solid line indicates a linear fit.

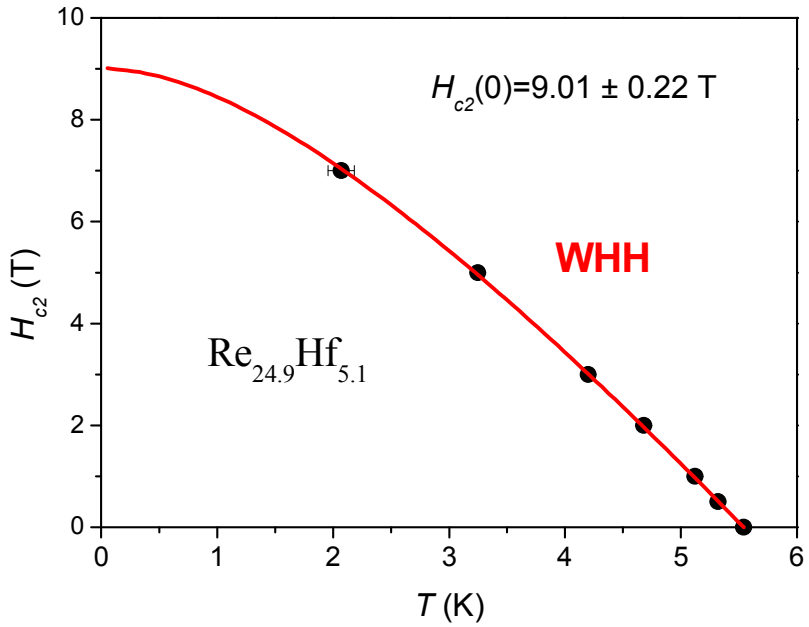

Figure 9 Temperature dependence of upper critical fields of $Re_{24.9}Hf_{4.1}$, and the red curve is from WHH theory.

From the behavior of specific heat, the order parameter will be *s*-wave, but, in the above introduction, we know the possible order parameter of non-centrosymmetric superconductors is two-gap or anisotropic gap from theatrical calculation. In order to ascertain which fitting is the best, we calculated the chi-square and presented the highly probable fitting results in Figure 10.

We present all the parameters are listed in Table III and Table IV. Even we can describe the specific heat as two-gap and anisotropic gap by the mathematically numerical analysis, but, does it have physical meaning? So, we have to check superconductor within which limit.

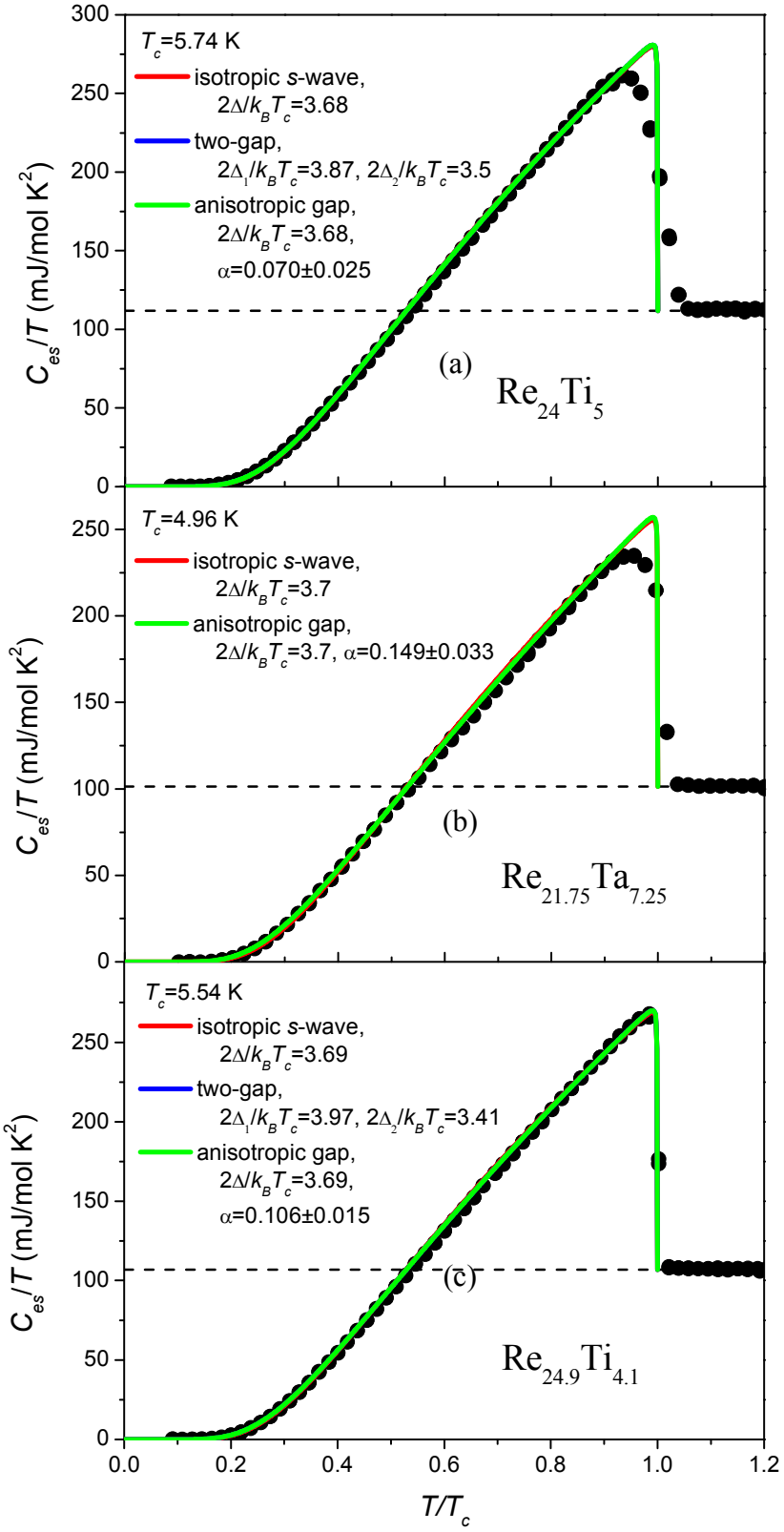

Figure 10 The black solid is superconducting electronic conurbation of (a)$Re_{24}Ti_5$, (b)$Re_{21.75}Ta_{7.25}$ and (c)$Re_{24.9}Hf_{4.1}$ with isotropic *s*-wave fitting(red line), two-gap fitting(blue line) and anisotropic fitting(light green light).

Table III: A comparison of several important parameters for non-centrosymmetric super-conductors with α-Mn structure.

Parameters		$Re_{24}Ti_5$	$Re_{21.75}Ta_{7.25}$	$Re_{24.9}Hf_{4.1}$
T_c [K]		5.74	4.96	5.54
γ_n [mJ/mol K^2]		111.8	101.3	107
θ_D [K]		343	325	335
$\Delta C/\gamma_n T_c$		1.60	1.52	1.55
λ_{ep}		0.45	0.32	0.37
$H_{c2}(0)$ [T]	*from* WHH	10.75	< 9	9.01 ± 0.22
	from $\gamma(H)$			9.84 ± 0.6
$-\frac{dH_{c2}}{dT}\Big\|_{T=T_c}$ [T/K]		2.7	< 2.61	2.34
ξ [Å]	*from* WHH	55.3	> 60.4	60.4 ± 0.7
	from $\gamma(H)$			57.8 ± 1.8

Table IV: The energy gap of fits.

Order parameter	$Re_{24}Ti_5$	$Re_{21.75}Ta_{7.25}$	$Re_{24.9}Hf_{4.1}$
Isotropic *s*-wave			
$2\Delta_s/k_BT_c$	3.68 ± 0.01	3.70 ± 0.07	3.69
Two-gap			
$2\Delta_s/k_BT_c$	3.68	---	3.69
$2\alpha\|\Delta_p\|/k_BT_c$	0.18		0.28
Anisotropic gap			
$2\Delta/k_BT_c$	3.68 ± 0.01	3.70	3.69
α	0.070 ± 0.025	0.149 ± 0.033	0.106 ± 0.015

Dirty or Clean Limit?

The Transport Measurements

The function of mean free path is $l = v_F\tau$, where v_F is the Fermi velocity and the relaxation time $\tau = m/\rho ne^2$ from Drude model. We used equation (2-6) to estimate Fermi energy ε_F, $7.08\ \text{eV}$ for $Re_{24}Ti_5$, $9.84\ \text{eV}$ for $Re_{21.75}Ta_{7.25}$, $7.13\ \text{eV}$ for $Re_{24.9}Hf_{4.1}$ and figure out the corresponding Fermi velocity $v_F = \sqrt{2\varepsilon_F/m} = 1.58 \times 10^8\ \text{cm/s}$, $1.86 \times 10^8\ \text{cm/s}$, and $1.58 \times 10^8\ \text{cm/s}$ respectively.

Then we used van der Pauw to measure the resistances and calculated their resistivity by equation (3-8), which reveals the relation to average resistance and thickness. After that, changing the configuration of samples and measuring the Hall coefficient, taking R_H for room temperature to derive the carrier concentration n. We observed that the Hall coefficient varies with the temperature, which is shown in Figure 13.

We estimated the mean free path l of our samples, which is listed in Table VI and shorter than coherence length ξ. It implies these superconductors within the contexts of dirty limit, in principle, the multi-gap fitting loses the physical meaning in this kind of situation.

Because the contributions of resistivity including impurity and grain boundary, assume the $H_{c2}(0) < 9\ \text{T}$ for $Re_{21.75}Ta_{7.25}$ and calculate its residual resistivity $\rho_{res} < 153.3\ \mu\Omega\ \text{cm}$ by the equation[23]:

$$-\left.\frac{dH_{c2}}{dT}\right|_{T=T_c} = 4.48 \times 10^4 \gamma_n \rho_{res}\ \text{Oe/K} \qquad (4\text{-}3)$$

In the same way, the residual resistivity of $Re_{24}Ti_5$ and $Re_{24.9}Hf_{4.1}$ are $144.1\ \mu\Omega$ and $130.6\ \mu\Omega$. The measured resistivity is in the same order with residual resistivity, the contribution to resistivity is almost from the residual resistivity.

Table V: Hall coefficient of non-centrosymmetric superconductors in the unit of cm^3/C.

Temperature	$Re_{24}Ti_5$	$Re_{21.8}Ta_{7.2}$	$Re_{24.9}Hf_{4.1}$
20 K	$(5.09 \pm 0.10) \times 10^{-5}$	$(2.86 \pm 0.46) \times 10^{-5*}$	$(1.17 \pm 0.58) \times 10^{-4}$
100 K	$(9.37 \pm 0.23) \times 10^{-5}$	$(3.11 \pm 0.39) \times 10^{-5}$	$(3.01 \pm 0.75) \times 10^{-5}$
200 K	$(7.76 \pm 0.28) \times 10^{-5}$	$(4.22 \pm 0.43) \times 10^{-5}$	$(4.10 \pm 0.99) \times 10^{-5}$
300 K	$(7.70 \pm 0.32) \times 10^{-5}$	$(4.45 \pm 0.34) \times 10^{-5}$	$(7.22 \pm 1.57) \times 10^{-5}$

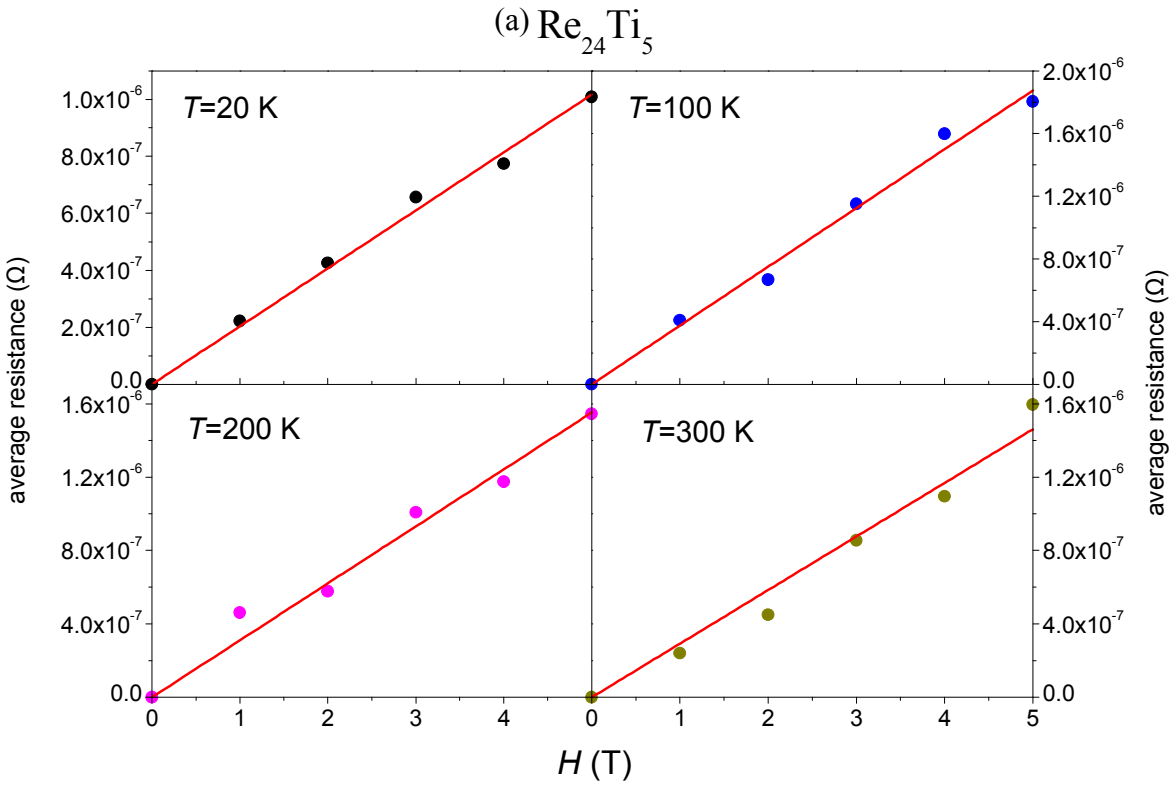

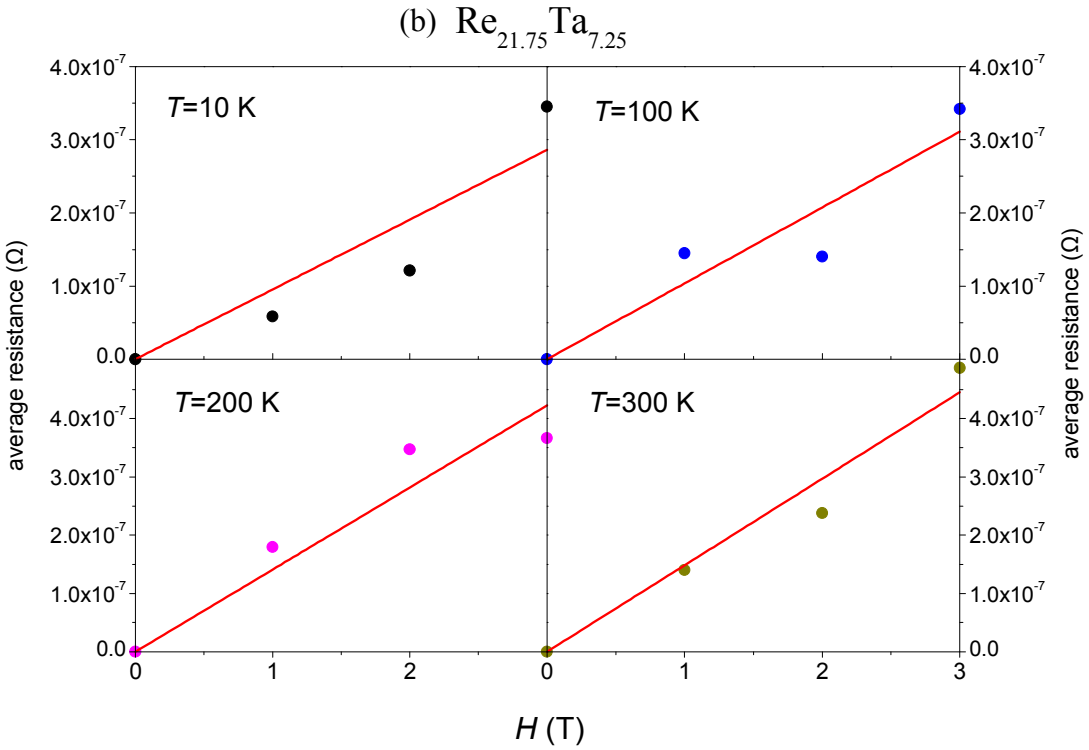

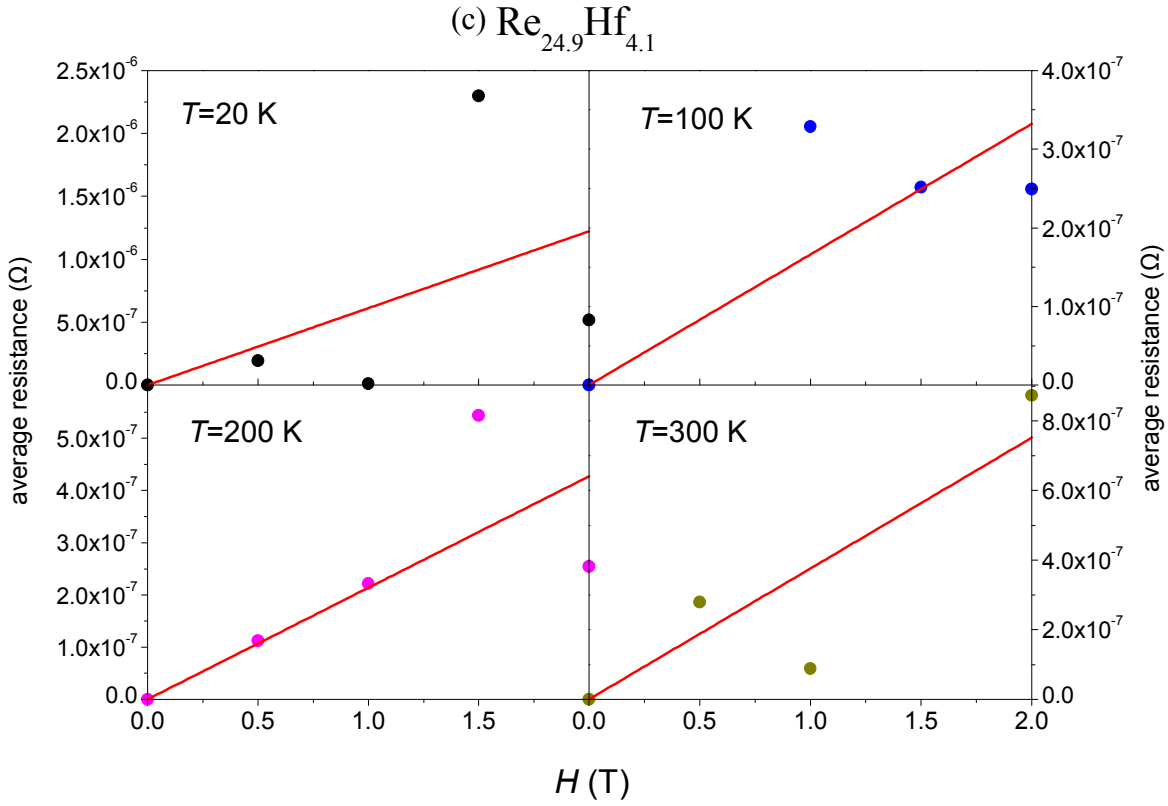

Figure 4-11 The Hall voltage *vs.* magnetic fields of (a)$Re_{24}Ti_5$, (b)$Re_{21.75}Ta_{7.25}$ and (c)$Re_{24.9}Hf_{4.1}$ with different temperatures.

Table VI: Several important parameters of non-centrosymmetric superconductors.

Parameter	$Re_{24}Ti_5$	$Re_{21.75}Ta_{7.25}$	$Re_{24.9}Hf_{4.1}$
$\rho(T = 20\ \mathrm{K})$ [μΩ cm]	125.5	136	148.9
ρ_{res} [μΩ cm]	144.06	< 153.3	130.56
n [cm^{-3}]	8.56×10^{22}	1.40×10^{23}	8.66×10^{22}
ε_F [eV]	7.08	9.84	7.13
τ [sec]	3.31×10^{-16}	1.86×10^{-16}	1.54×10^{-16}
l [Å]	5.23	3.46	2.43
$H_{c2}(0)$ [T]	10.75	< 9	9.01 ± 0.22
$-H'_{c2}\|_{T=T_c}$ [T/K]	2.7	< 2.61	2.34
ξ [Å]	55.3	> 60.4	60.4 ± 0.7
dirty/clean limit	dirty limit	dirty limit	dirty limit

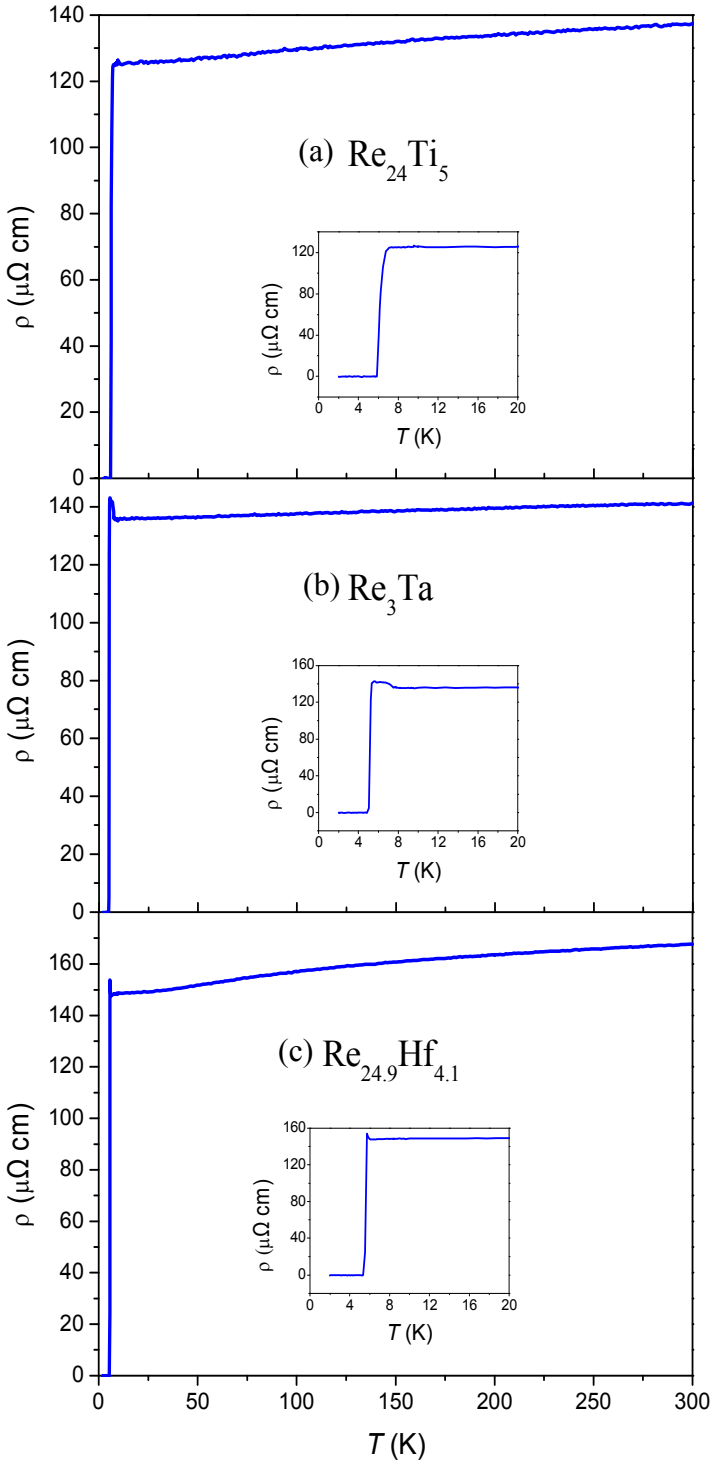

Figure 12 The resistivity *vs.* temperature of (a)$Re_{24}Ti_5$, (b)$Re_{21.75}Ta_{7.25}$, and (c)$Re_{24.9}Hf_{4.1}$.

Insert: zoom in the lower temperature region.

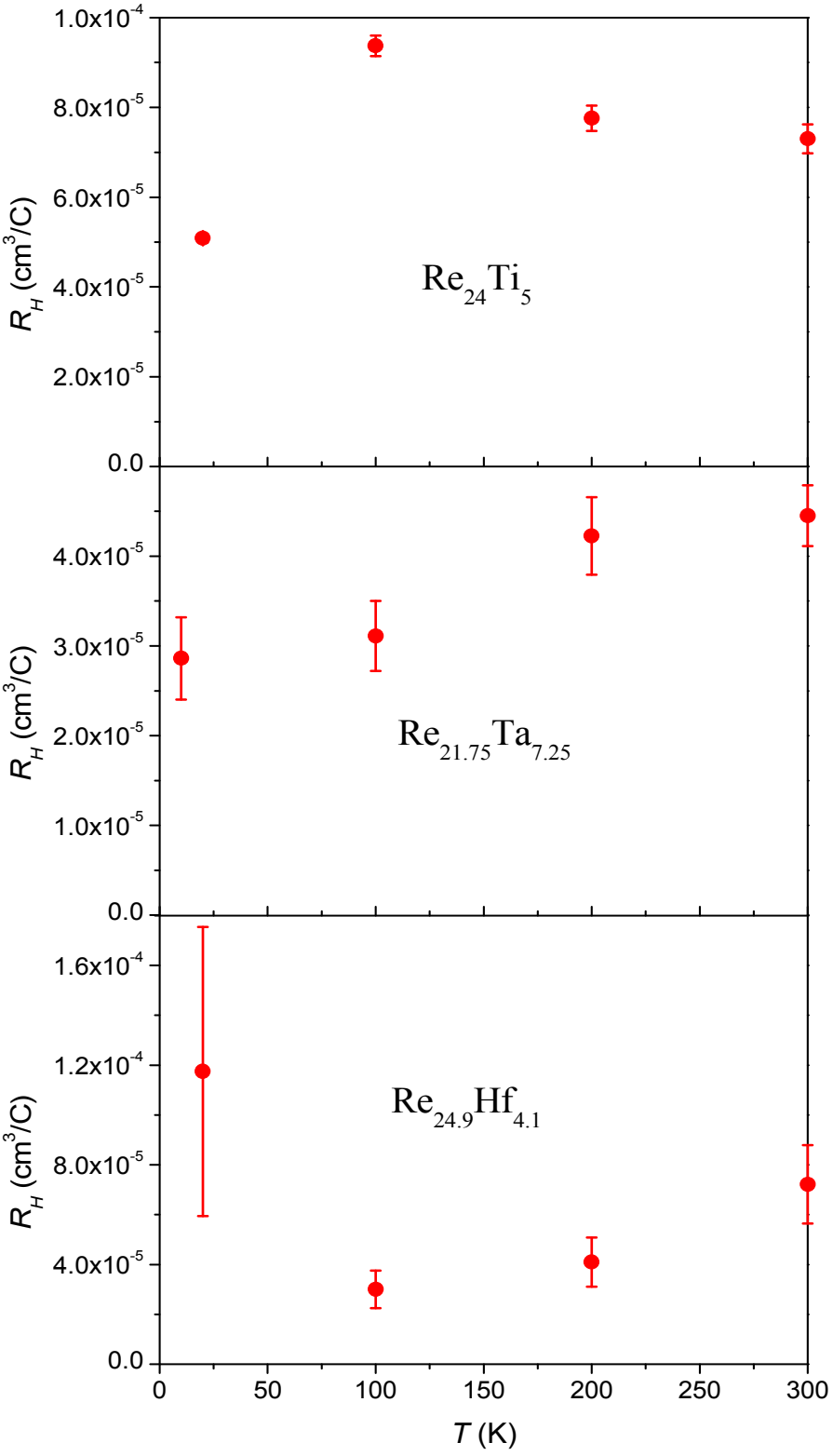

Figure 13 Hall coefficient *vs.* temperature of (a)$Re_{24}Ti_5$, (b)$Re_{21.75}Ta_{7.25}$, and (c)$Re_{24.9}Hf_{4.1}$.

The Case of MgB_2

One of its specific heat measurements points it out that MgB_2 cannot be defined by single gap and its magnetic field dependence of electronic specific heat coefficient $\gamma(H)$ is not proportion to H or $\sqrt{H}$[26]. All the evidences reveal that MgB_2 is the multigap nature of the superconducting state. Although multigap superconductor should be clean limit, MgB_2 proved to be in the dirty limit[24][25]. Obviously, our fittings would be a reference. There is no denying that our samples may be two-gap or anisotropic gap.

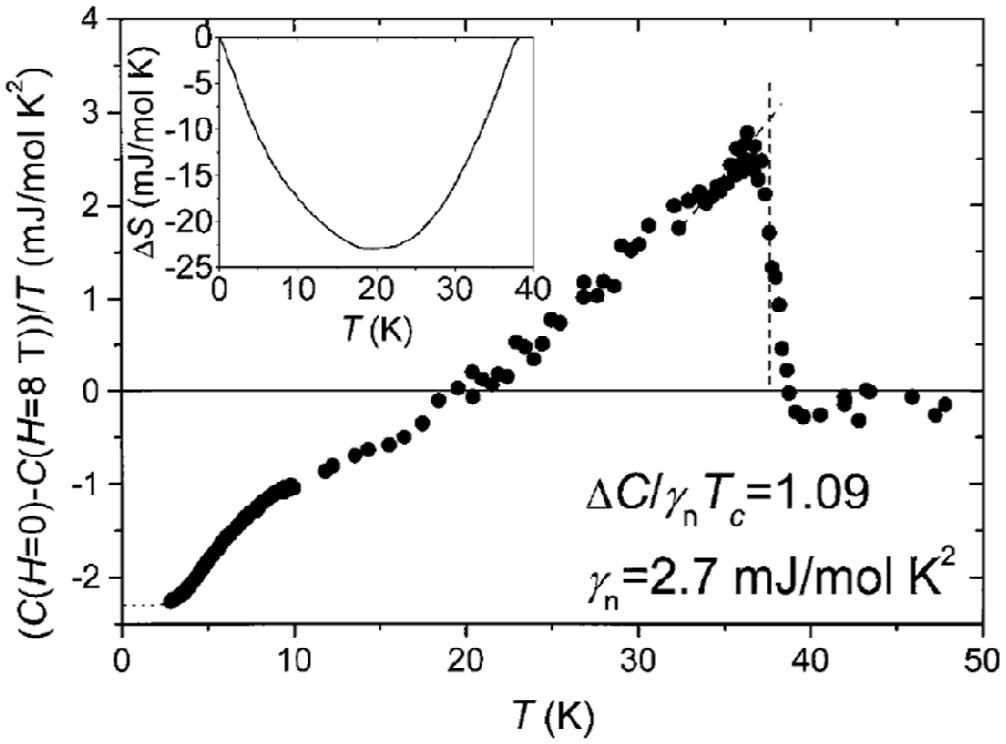

Figure 14 $\Delta C/T$ *vs.* T. The dashed lines are determined by the conservation of entropy around the anomaly and used to estimate $\Delta C/T_c$.

Inset: Entropy difference ΔS by integration of $\Delta C/T$ according to the extended dot line[26].

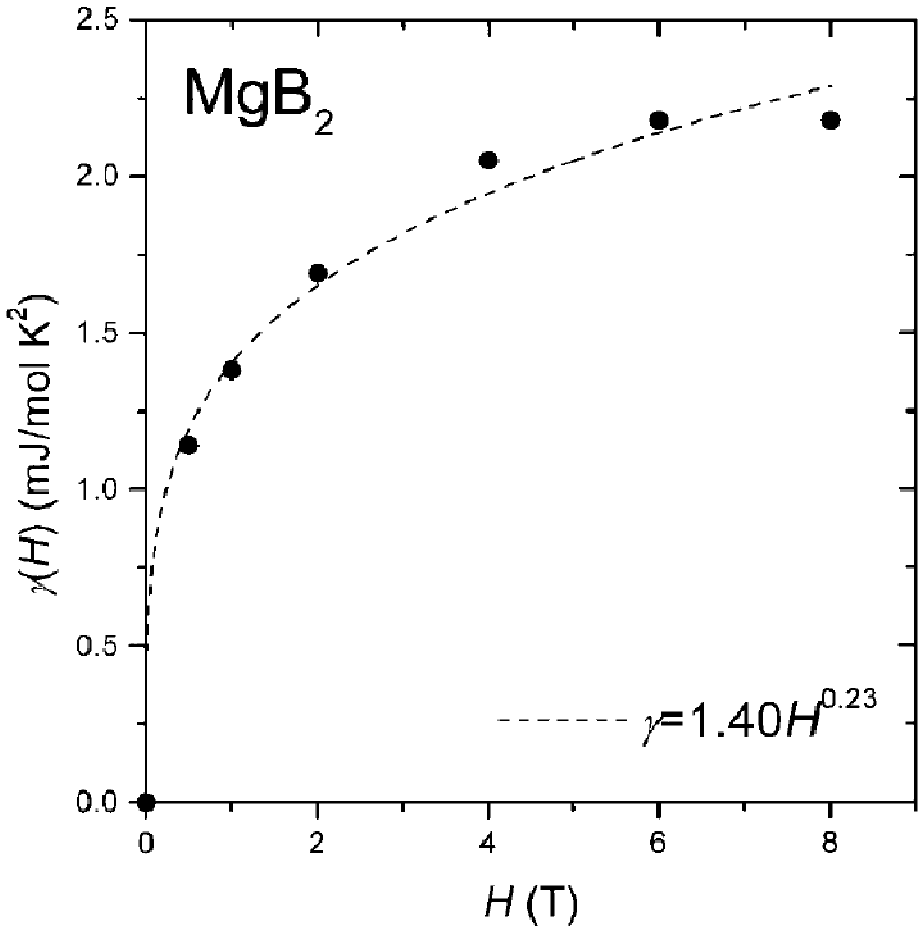

Figure 15 The magnetic field dependence of $\gamma(H)$. The dashed line is a fit to the power law[26].

參考文獻

[1] M. Yogi, Y. Kitaoka, S. Hashimoto, T. Yasuda, R. Settai, T. D. Matsuda, Y. Haga, Y. Ōnuki, P. Rogl, and E. Bauer, Phys. Rev. Lett. 92, 027003 (2004).

[2] P. A. Frigeri, D. F. Agterberg, A. Koga, and M. Sigrist, Phys. Rev. Lett. 92, 097001 (2004).

[3] K. Izawa, Y. Kasahara, Y. Matsuda, K. Behnia, T. Yasuda, R. Settai, and Y. Onuki, Phys. Rev. Lett. 94, 197002 (2005).

[4] I. Bonalde, W. Brämer-Escamilla, and E. Bauer, Phys. Rev. Lett. 94, 207002 (2005).

[5] Serdar Sakarya, William Knafo, Niels H. Van Dijk, Yingkai Huang, Karel Prokes, Christoph Meingast, and Hilbert Von Löhneysen, Journal of the Physical Society of Japan 76, 014702 (2007).

[6] Rikiya Yoshida, Hiroyuki Okazaki, Keisuke Iwai, Kengo Noami, Takayuki Muro, Mario Okawa, Kyoko Ishizaka, Shik Shin, Zheng Li, Jianlin Luo, Guo-qing Zheng,

Tamio Oguchi, Masaaki Hirai, Yuji Muraoka, and Takayoshi Yokoya, Journal of the Physical Society of Japan 78, 034705 (2009).
[7] K. Tahara, Z. Li, H. X. Yang, J. L. Luo, S. Kawasaki, and Guo-qing Zheng, Phys. Rev. B 80, 060503(R) (2009).
[8] A. B. Karki, Y. M. Xiong, N. Haldolaarachchige, S. Stadler, I. Vekhter, P. W. Adams, D. P. Young, W. A. Phelan and Julia Y. Chan, Phys. Rev. B 83, 144525 (2011).
[9] P. K. Biswas, M. R. Lees, A. D. Hillier, R. I. Smith, W. G. Marshall, and D. McK. Paul, Phys. Rev. B 84, 184529 (2011).
[10] P. K. Biswas, A. D. Hillier, M. R. Lees, and D. McK. Paul, Phys. Rev. B 85, 134505 (2012).
[11] C. S. Lue, T. H. Su, H. F. Liu, and Ben-Li Young, Phys. Rev. B 84, 052509 (2011).
[12] E. Bauer, G. Rogl, Xing-Qiu Chen, R. T. Khan, H. Michor, G. Hilscher, E. Royanian, K. Kumagai, D. Z. Li, Y. Y. Li, R. Podloucky, and P. Rogl, Phys. Rev. B 82, 064511 (2010).
[13] A. B. Karki, Y. M. Xiong, I. Vekhter, D. Browne, P. W. Adams, D. P. Young, K. R. Thomas, Julia Y. Chan, H. Kim and R. Prozorov, Phys. Rev. B 82, 064512 (2010).
[14] C. N. Kuo, H. F. Liu, and C. S. Lue, Phys. Rev. B 85, 052501 (2012).
[15] C. S. Lue, H. F. Liu, C. N. Kuo, P. S. Shih, J.-Y. Lin, Y. K. Kuo, M. W. Chu, T.-L. Hung and Y. Y. Chen, Supercond. Sci. Technol. 26, 055011 (2013).
[16] V. Z. Kresin and V. P. Parkhomenko, Sov. Phys. Solid State 16, 2180 (1975).
[17] K. Sugawara, T. Sato, S. Souma, T. Takahashi, and A. Ochiai, Phys. Rev. B 76, 132512 (2007).
[18] J. Chen, M. B. Salamon, S. Akutagawa, J. Akimitsu, J. Singleton, J. L. Zhang, L. Jiao, and H. Q. Yuan, Phys. Rev. B 83, 144529 (2011).
[19] T. Klimczuk, F. Ronning, V. Sidorov, R. J. Cava, and J. D. Thompson, Phys. Rev. Lett. 99, 257004 (2007).
[20] I. Bonalde, R. L. Ribeiro, W. Brämer-Escamilla, G. Mu and H. H. Wen, Phys. Rev. B 79, 052506 (2009).
[21] C.W.J. Beenakker, Annu. Rev. Condens. Matter Phys. 4, 113 (2013).
[22] Jason Alicea, Rep. Prog. Phys. 75, 076501 (2012).
[23] T. P. Orlando, E. J. McNiff, Jr., S. Foner, and M. R. Beasley, Phys. Rev. B 19, 4545 (1979).
[24] A. E. Koshelev, A. A. Golubov, Phys. Rev. Lett. 90, 177002 (2003).
[25] A. Gurevich, S. Patnaik, V. Braccini, K. H. Kim, C. Mielke, X. Song, L. D. Cooley, S. D. Bu, D. M. Kim, J. H. Choi, L. J. Belenky, J. Giencke, M. K. Lee, W. Tian, X. Q. Pan, A. Siri, E. E. Hellstrom, C. B. Eom and D. C. Larbalestier, Supercond. Sci. Technol. 17, 278 (2004).

[26] H. D. Yang, J.-Y. Lin, H. H. Li, F. H. Hsu, C. J. Liu, S.-C. Li, R.-C. Yu, and C.-Q. Jin, Phys. Rev. Lett. 87, 167003 (2003).